Surface & Coatings Technology 478 (2024) 130483

Contents lists available at ScienceDirect

Surface & Coatings Technology

journal homepage: www.elsevier.com/locate/surfcoat

Full length article

Effect of different galvanic coupling methods on the surface chemical transformation of TC4 titanium alloy

YaJun Li [a], Wenhua Xu [b], Ningbo Li [c], Zhen Ma [a], Baoxu Huang [a], Jie Ma [a], Hui Chen [a], Xuehui Hao [a], Xingchuan Zhao [a,*]

[a] School of Materials Science and Engineering, Liaocheng University, Liaocheng 252059, China
[b] School of Materials Science and Engineering, Shandong University, Ji'nan 250061, China
[c] Department of Stomatology, Shandong Provincial Hospital Affiliated to Shandong First Medical University, Shandong First Medical University, Ji'nan 250021, China

ARTICLE INFO

Keywords:
TC4 titanium alloy
Galvanic coupling phosphate chemical conversion
Hopeite
Magnetron sputtering multipoint coupling

ABSTRACT

In clinical applications, titanium and its alloy implants often suffer from corrosion, wear and tear, and poor biological activity. Surface modification is critical for improving the stability and bioactivity of titanium and its alloys. Zinc phosphate chemical conversion has received increasing attention as a promising technique for biomedical applications. However, the presence of a passive oxide layer on the TC4 (Ti6Al4V) surface poses challenges for conventional chemical conversion methods. In this study, the principle of galvanic coupling was utilized to facilitate the surface chemical transformation of TC4 titanium alloy, referred to as galvanic coupling phosphate chemical conversion (GCPCC). The effects of two types of galvanic coupling and different plastic deformations on the surface chemical transformation of TC4 titanium alloy at different temperatures were mainly investigated. The results indicate that the Ti/Fe multipoint coupling formed by magnetron sputtering during chemical transformation at 70 °C significantly enhances the nucleation sites of hopeite ($Zn_3(PO_4)_2{\cdot}4H_2O$) and accelerates the nucleation rate. Compared with line-coupled conversion coatings, multipoint coupling GCPCC coatings exhibit superior uniformity and finer microstructure, and the thickness of the laths is significantly reduced from 5 to 10 μm to less than 1 μm. Moreover, the temperature exerts a substantial influence on the formation of conversion coatings. At 70 °C, the GCPCC coating primarily comprises hopeite, while the coating resulting from chemical conversion treatment consists of both hopeite and an amorphous ZnP-like granular coating at 50 °C.

1. Introduction

Titanium and its alloys have extensive applications in the field of medicine due to their favourable properties, including a low coefficient of thermal expansion, excellent corrosion resistance, and elastic modulus similar to human bones [1,2]. These materials are commonly employed in medical implants to replace or support damaged tissue structures, such as bones, joints, teeth, heart valves, and bone fixation devices [3–5]. Among titanium alloys, Ti6Al4V (TC4) has been widely applied in clinical medicine. However, the inherent inert oxide coating on the surface of TC4 alloy results in limited biological activity [6,7], hindering the growth of bone tissue and cells following implantation in the human body [8,9]. Therefore, it is necessary to improve the biological activity of TC4 through surface modification [10–12]. Furthermore, the naturally formed oxide coating on the TC4 alloy surface is relatively thin. After TC4 alloy is implanted into the human body, long-term exposure to body fluids and proteins can lead to wear and corrosion on the surface of the TC4 alloy implant, potentially causing particle detachment and ion release [13,14].

Notably, the release of toxic ions such as aluminium (Al) and vanadium (V) from TC4 alloys can have adverse effects on human health and bone healing. The long-term stability of titanium alloy implanted in the human body can be guaranteed by improving the corrosion resistance and biocompatibility of the titanium alloy surface. Surface modification treatment is reasonable, and enhancing both biological activity and stability represents a challenging and vital aspect of ongoing research regarding titanium surface modification [15,16].

Hopeite is an inorganic material with low solubility and good biocompatibility when exposed to biological environments [17,18]. Zinc is not only an essential element for proteins but also participates in

* Corresponding author.
E-mail address: zhaoxingchuan@lcu.edu.cn (X. Zhao).

https://doi.org/10.1016/j.surfcoat.2024.130483
Received 13 November 2023; Received in revised form 3 January 2024; Accepted 26 January 2024
Available online 28 January 2024

the synthesis of various enzymes. Research findings have shown that zinc is involved in many physiological processes and metabolic pathways in the human body [19,20]. Furthermore, zinc has antimicrobial properties, showcasing its resistance against a wide array of both prokaryotic and eukaryotic bacteria [21–23]. It is noteworthy that the addition of zinc, as an essential element, is less toxic and safer for biomaterials than the addition of silver.

Chemical conversion is the process involving the induction of chemical reactions within metals immersed in an electrolyte to form insoluble inorganic thin coatings. This conversion coating grows in situ and has a relatively strong adhesion to the substrate [24–26]. Moreover, this conversion technology has advantages such as rapid coating formation and simple operation [27–30], so it has found wide application in the surface modification of steel, magnesium alloys and other materials. However, there are few studies on the chemical transformation of the surface of titanium and its alloys. This transformation occurs because the naturally occurring oxide layer impedes the growth or in situ deposition of insoluble phosphates on the surface of titanium and its alloy in a solution. Therefore, it is difficult to generate a stable conversion coating on the surface of titanium alloys using traditional chemical conversion processes. Some prior studies have utilized high-temperature and long-term hydrothermal treatment to increase the nucleation and growth energy of titanium surfaces to prepare hopeite coatings [31,32]. Although this method offers some improvement in chemical conversion, the lengthy processing times and rigorous conversion conditions make it unsuitable for large titanium alloys. Alternatively, some researchers have employed iron clips to trigger coating formation through point contact electrical coupling, but this approach can lead to uneven grain sizes and coating thicknesses.

Due to the electrochemical potential difference between dissimilar metals, galvanic couples are formed in the chemical conversion solution, leading to the transport of ions and electrons between these metals, resulting in electrochemical reactions and galvanic corrosion. For inert metals such as titanium alloys, galvanic corrosion can promote the formation of conversion coatings during surface modification [33]. In this experiment, the dissimilar metal galvanic coupling method was employed to assist the chemical transformation. The control group used iron strips in direct contact with TC4 for coupling, while the experimental group employed magnetron sputtering to evenly distribute iron in a point-like manner on the surface of the TC4 titanium alloy, establishing it as a coupling pair for coupling with TC4. Then, the influence of coupling methods on the morphology, structure, and performance of the chemical conversion coating on the surface of the TC4 alloy was explored. Meanwhile, considering that the TC4 alloy substrate itself also has an influence on the chemical transformation, the effects of different plastic deformation methods of titanium alloys on their chemical transformations were further investigated. In this study, a detailed mechanism of coating formation induced by galvanic coupling of iron and titanium alloy has been proposed.

2. Experimental section

2.1. Materials and pretreatment

Commercial TC4 was cut into disks (φ11 × 3 mm) for substrate. The TC4 sheets were abraded and polished with 240#, 360#, 480#, 600#, 800# and 1200# emery paper, followed by ultrasonic cleaning in acetone, ethanol and deionized water, respectively. Acid etching and surface activation were carried out by immersing the discs in hydrofluoric acid (HF, 2 %) and Ti colloid ($Na_4TiO(PO_4)_2$, 3 g/L) solutions for 30 s at room temperature. After that, the as-pretreated TC4 disks were immersed in designed GCPCC solutions to conduct chemical reactions at 50 °C and 70 °C for 10 min and 30 min. According to the degree of deformation, the disks were denoted as undeformed (UD), tensile (TD) and compression (CD).

Table 1
Compositions of the GCPCC Solutions.

Composition	H_3PO_4	HNO_3	ZnO	Ca $(NO_3)_2{\cdot}4H_2O$	Accelerants
Concentration	10 mL/L	30 mL/L	25 g/L	5 g/L	7.5 g/L

2.2. Galvanic coupling phase chemical conversion process

The compositions of the GCPCC solutions are listed in Table 1. This experiment expanded on the "active center" theory to increase the concentration of Fe^{2+} by adding reducing iron powder, promote the nucleation of hopeite, and significantly improve the conversion efficiency. Consequently, the chemical conversion solution underwent iron powder ageing treatment, which involves adding 5 g of Fe powder to the preconfigured conversion solution and allowing it to stand for 24 h before filtering out. Finally, the pH value of the chemical conversion solution was adjusted to 2.6.

Galvanic coupling determines the coupling cathode and anode based on the level of their respective corrosion potentials. Typically, the component with a lower corrosion potential is used as the anode, while the component with a higher corrosion potential serves as the cathode. In this experiment, Fe is used as the coupling anode and the TC4 coupling cathode. The coupling between the metal Fe and the TC4 alloy substrate is recorded as Ti/Fe to accelerate the dissolution of the substrate material in the conversion solution to accelerate the formation of the conversion coating on the surface.

To investigate the influence of different contact methods on the conversion coating in the chemical conversion process, two ways of coupling TC4 alloy with iron featuring different plastic deformations were investigated. These methods included the combination of linear iron and TC4 as Ti/Fe-L through line coupling and uniform iron sputtering with multiple-point distribution on the surface of TC4 alloy as Ti/Fe-F through magnetron sputtering. The experiments were conducted to explore the nucleation and distribution of hopeite under different coupling methods with a specific emphasis on analysing the structure and properties of the chemical conversion coating layer formed at a temperature of 50 °C.

2.3. Characterization

Sample morphologies were investigated by scanning electron microscopy (SEM, Zeiss, Germany), and the elemental composition and distribution of the samples were determined with an energy-dispersive X-ray spectrometer (EDS) attached to the SEM. The acceleration voltage during the FE-SEM and EDS tests was 15 kV. The phase composition was observed through an X-ray diffractometer (XRD, Smartlab, Rigaku, Japan) equipped with CuKα radiation at measurement steps of 0.01°. Surface roughness measurements and morphological characterization of the samples were performed using an optical three-dimensional (3D) surface profiler (SuperView W3, CHOTEST, China). The morphology and crystal structure of the coated samples were further examined using high-resolution transmission electron microscopy (HRTEM, FEI Tecnai F30, America). X-ray photoelectron spectroscopy (XPS, Thermo Escalab xi+, America) with Al Kα radiation was used to investigate the chemical states of the samples. In addition, the functional groups of the GCPCC coating were characterized using a Fourier transform infrared spectrometer (FTIR, IR100, Nicolet, America), and the tested spectrum ranged from 4000 to 400 cm^{-1}.

2.4. Surface abrasion resistance test

The friction and wear tests were carried out using an MFT-EC4000 reciprocating friction and wear tester, which was equipped with GCr15 grinding balls (φ = 5 mm). The normal loads were 2 N and 5 N for a test duration time of 30 min, the reciprocating distance was 5 mm with

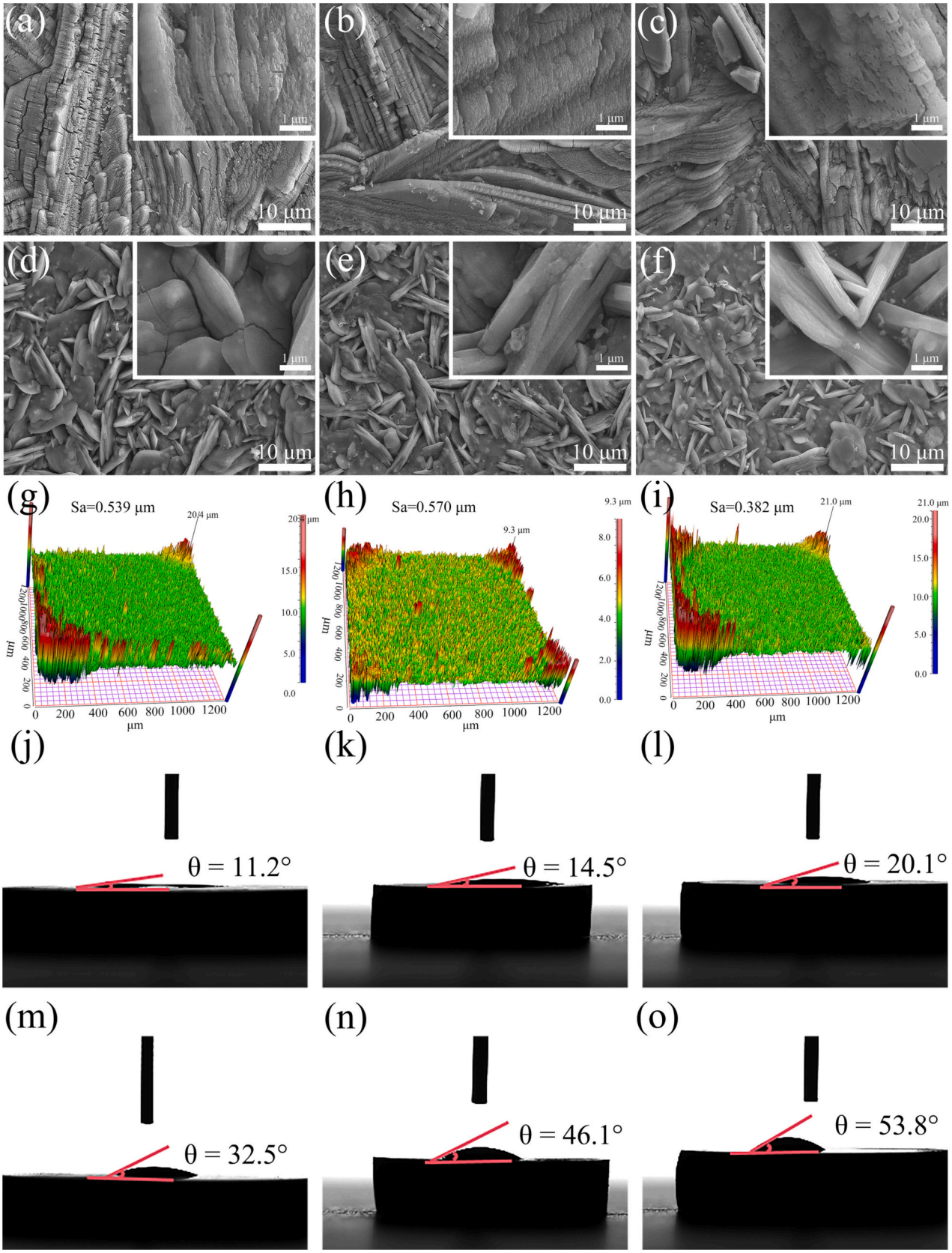

Fig. 1. SEM images, optical 3D profile images and water contact angles of the GCPCC coatings treated at 70 °C for 30 min. (a) UD Ti/Fe-L, (b) TD Ti/Fe-L, (c) CD Ti/Fe-L, (d) UD Ti/Fe-F, (e) TD Ti/Fe-F, (f) CD Ti/Fe-F, (g) UD Ti/Fe-F, (h) TD Ti/Fe-F, (i) CD Ti/Fe-F, (j) UD Ti/Fe-L, (k) TD Ti/Fe-L, (l) CD Ti/Fe-L, (m) UD Ti/Fe-F, (n) TD Ti/Fe-F, (o) CD Ti/Fe-F.

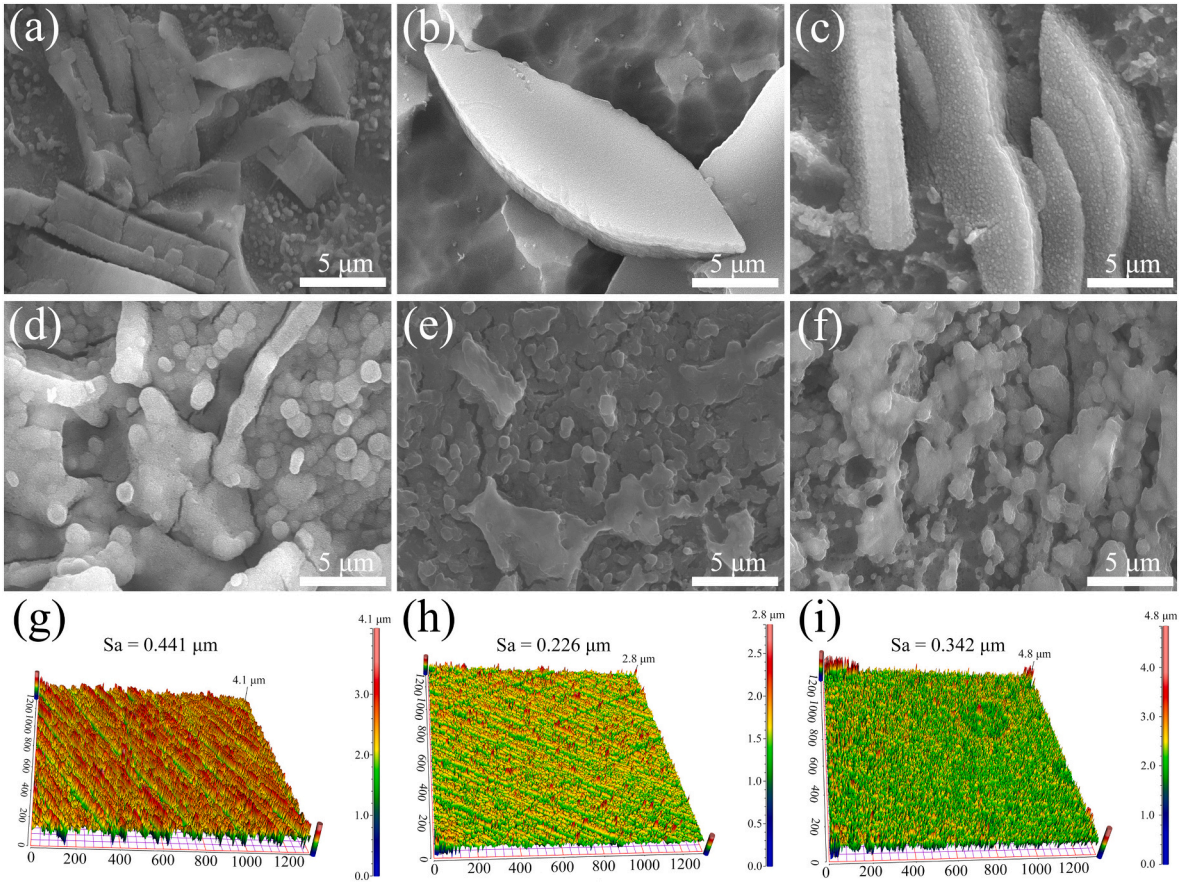

Fig. 2. SEM images and optical 3D profile images of the GCPCC coatings treated at 50 °C for 30 min. (a) UD Ti/Fe-L, (b) TD Ti/Fe-L, (c) CD Ti/Fe-L, (d) UD Ti/Fe-F, (e) TD Ti/Fe-F, (f) CD Ti/Fe-F, (g) Bare TC4, (h) CD Ti/Fe-L, (i) CD Ti/Fe-F.

a frequency of 2 Hz, and each test was repeated three times for each sample.

2.5. Electrochemical evaluation

The corrosion resistance of the samples was tested in 0.9 % NaCl with an Autolab PGSTAT302 electrochemical workstation with a three-electrode system. The potentiodynamic polarization curves were measured at a scanning rate of 1 mV/s at −0.5 V to 0.5 V vs. OCP (open circuit potential). Electrochemical impedance spectroscopy (EIS) measurements were performed under the stable state of OCP with a voltage disturbance amplitude of 5 mV and a frequency range from 100 kHz to 10 mHz.

3. Results and discussion

3.1. Effect on morphology and phase structure

Fig. 1 shows SEM images of the conversion coating formed by galvanic coupling chemical transformation on the surface of the TC4 alloy with different plastic deformations at 70 °C. The surface of TC4 under different conditions formed a chemical conversion coating that completely covered the substrate. However, there were clear distinctions in the characteristics of these coatings.

The conversion coating formed by the Ti/Fe-L group exhibited a larger particle size than that of the Ti/Fe-F group, and the crystal morphology of the Ti/Fe-L group conversion coating was significantly different from that of the Ti/Fe-F group. The Ti/Fe-L group conversion coating was composed of thick laths with a length of approximately 60–80 μm and a width of 5–10 μm, while the Ti/Fe-F group conversion coating was composed of fine lamellar crystals with a thickness of less than 1 μm. The reason for the different crystal morphologies is that magnetron sputtering increases the contact area between the ferroelectric couple and TC4, resulting in an increased number of nucleation sites of the conversion coating, thus yielding finer and denser grains. Fig. 1(g)-(i) shows the topographical features of the three Ti/Fe-F coatings. The optical 3D images reveal that GCPCC treatments under different conditions can change the topographical features of the TC4 surface. The topography fluctuates to different degrees due to the variation in crystal morphology and size.

The contact angles (θ) of coatings in Fig. 1(a)-(f) with distinct microstructures were measured using a sessile drop method to assess the wettability variations associated with crystal morphology, as depicted in Fig. 1(j)-(o). Surface wettability properties are typically influenced by the material's surface structure and surface free energy, with the θ value serving as an indicator of material wettability. Generally, materials with $\theta < 90°$ exhibit good hydrophilicity. In this experiment, different crystal morphologies were observed in coatings of samples subjected to line-coupled versus multi-point coupling after chemical transformation, resulting in a significant difference in contact angle. The multi-point coupled sample showed relatively poor wettability based on the θ value. However, both coupling methods yielded samples with θ values less than 90°, indicating hydrophilicity. In the realm of biomaterials, a material's hydrophilic ability is a critical criterion for its suitability as an implant material. A material with excellent hydrophilicity promotes cell adhesion and growth after implantation in the human body, thereby enhancing its compatibility with human tissues.

Fig. 2 shows SEM images of the conversion coating formed by galvanic coupling chemical transformation on the surface of the TC4 alloy with different plastic deformations at 50 °C. Notably, the line-

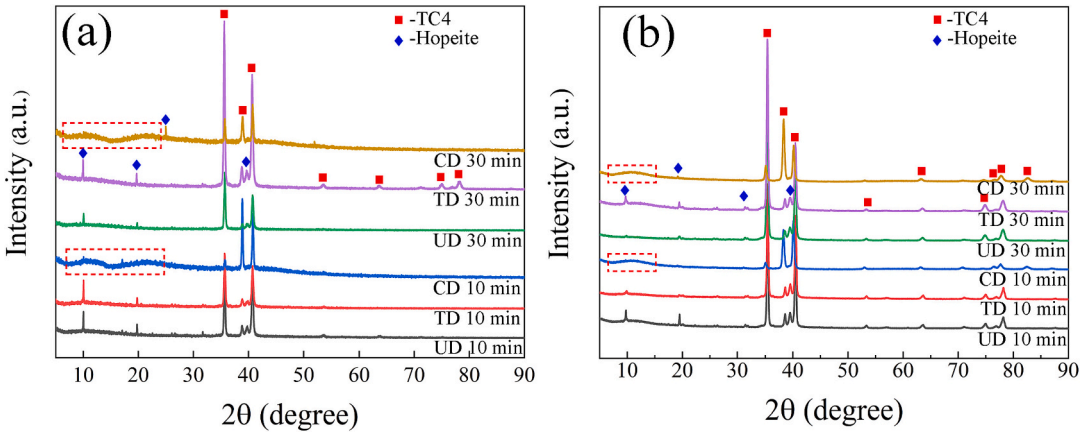

Fig. 3. XRD patterns of the GCPCC samples treated at 50 °C for 10 min and 30 min. (a) Ti/Fe-L, (b) Ti/Fe-F.

coupled conversion coating exhibits a lamellar structure. Compared with the conversion coating formed at 70 °C in Fig. 1, the crystal particle size of the conversion coating formed by the Ti/Fe-L group at 50 °C is considerably smaller, and the formed conversion coating is not complete enough to fully cover the TC4 substrate. This is because the conversion temperature can affect the chemical and electrochemical reactions at the interface between the metal and the solution during the conversion process, thereby significantly affecting the conversion rate [34]. Fig. 2 (g)-(i) shows the topographical features of bare TC4 and two types of compressed sample coatings. A typical parallel arrangement of scratch grooves can be seen on the surface of bare TC4, while the coated TC4 shows hill-like bulge topography.

Under certain other conditions, the relationship between the formation rate of the conversion coating and the conversion temperature adheres to the Arrhenius empirical formula, $\nu = Ae^{-E/RT}$ (ν represents the coating formation rate, A is the frequency factor, E is the reaction activation energy, T is the transformation temperature (K), and R is the gas constant.) [35]. Chemical conversion is an endothermic process, and increasing the temperature is beneficial to chemical conversion [36]. Conversely, the growth kinetics of the conversion coating are notably sluggish, and a complete coating cannot be formed at lower temperatures. However, lower temperatures are beneficial when studying the distribution of the initial nucleation of the coating layer. It is important to highlight that the morphology of the conversion coating formed by Ti/Fe-F is obviously different from that of Ti/Fe-L. The morphology of the surface conversion coating is similar to that of the amorphous state. Research has demonstrated that during the early stage of the formation of the chemical conversion coating, amorphous deposition takes place on the metal surface [37].

Fig. 3 shows the XRD patterns of the conversion coatings obtained under different treatment conditions at a conversion temperature of 50 °C. It can be seen that the main component of the coating after chemical conversion is the hopeite phase, and the main phase composition of the coating remains consistent with increasing conversion time. By comparing the relative intensities of hopeite crystal diffraction peaks in Fig. 3(a) and (b), it is found that in addition to the compressed sample, the intensity of hopeite diffraction peaks of the Ti/Fe-L and Ti/Fe-F conversion coatings decreases as the conversion time extension. This is because the formed conversion coating crystals redissolve over prolonged conversion time. This phenomenon is closely related to the coupling method. Both line coupling and multi-point coupling increase the contact area of Ti/Fe coupling, leading to a higher growth rate of the hopeite in a shorter timeframe. As the conversion time prolongs, the hopeite dissolves, and the rate of the newly grown hopeite is slower than its dissolution rate, resulting in a decrease in the relative intensity of hopeite diffraction peaks as the conversion time increases. This observation indicates that Ti/Fe-L and Ti/Fe-F contact methods are beneficial for improving conversion efficiency, and also indicates that there is a certain limit to the growth of conversion coating crystals, which is not proportional to time. In addition, it was observed that under different contact methods, the conversion coatings of all compressed TC4 samples contained a minor amount of hopeite phase, but the diffraction peaks were relatively weak, indicating that the growth rate of hopeite crystals after chemical conversion of compressed TC4 at 50 °C is slow relatively.

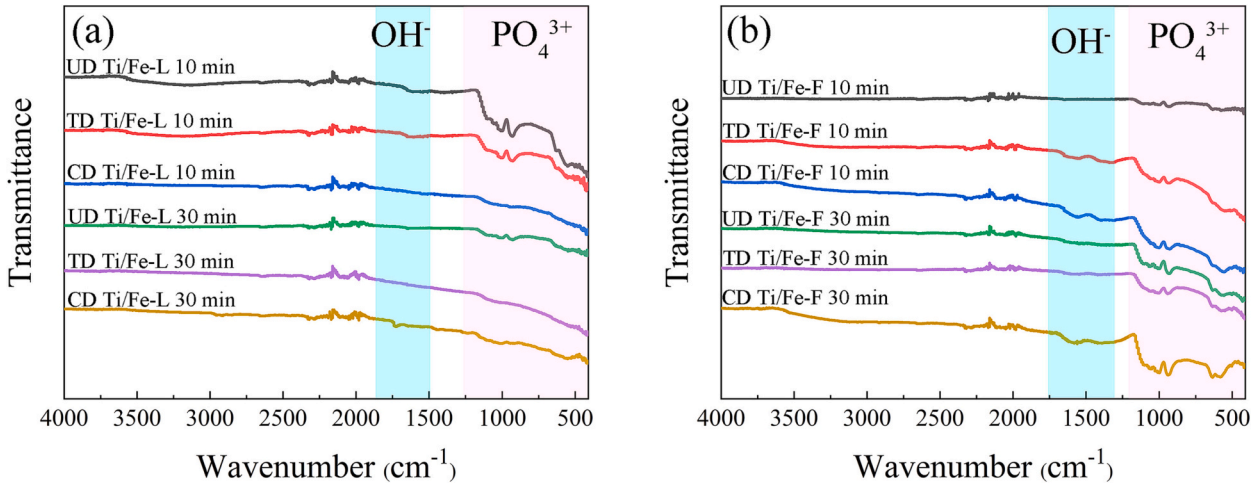

Fig. 4. FTIR spectra of the GCPCC samples treated at 50 °C for 10 min and 30 min. (a) Ti/Fe-L, (b) Ti/Fe-F.

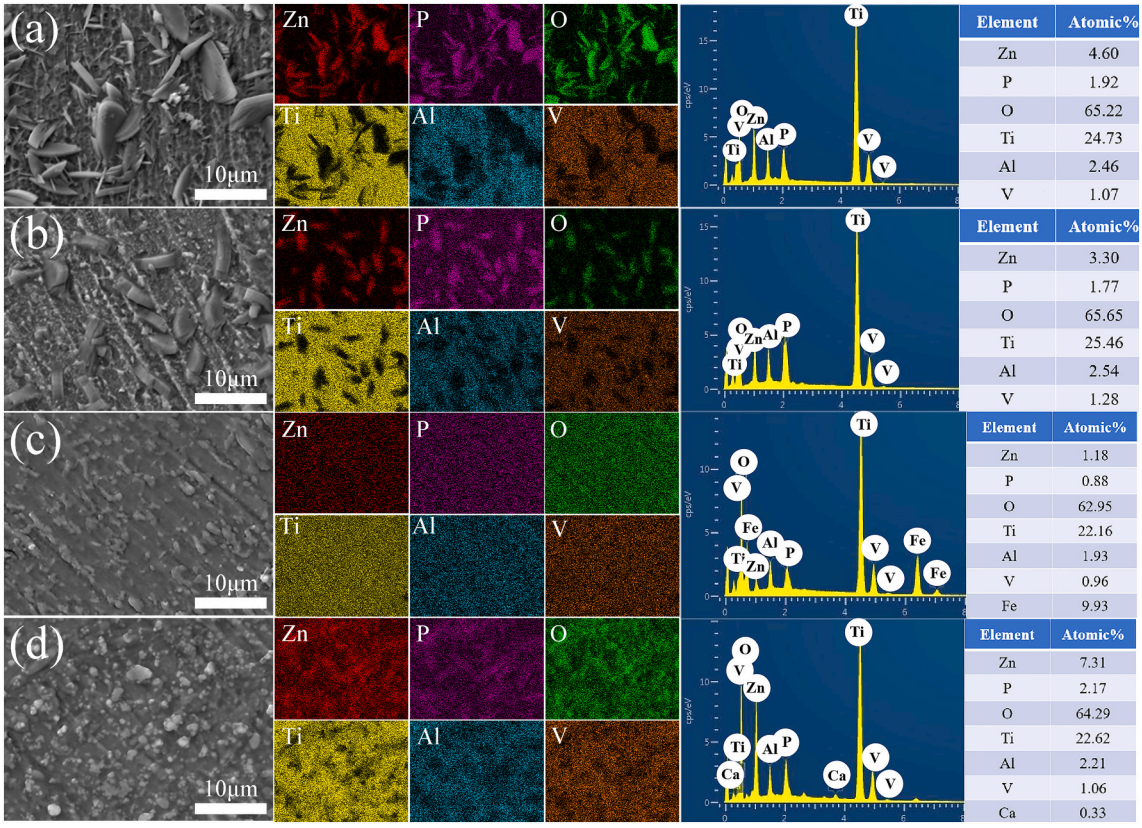

Fig. 5. EDS mappings of the different GCPCC samples. (a) TD Ti/Fe-L, (b) CD Ti/Fe-L, (c) TD Ti/Fe-F, (d) CD Ti/Fe-F.

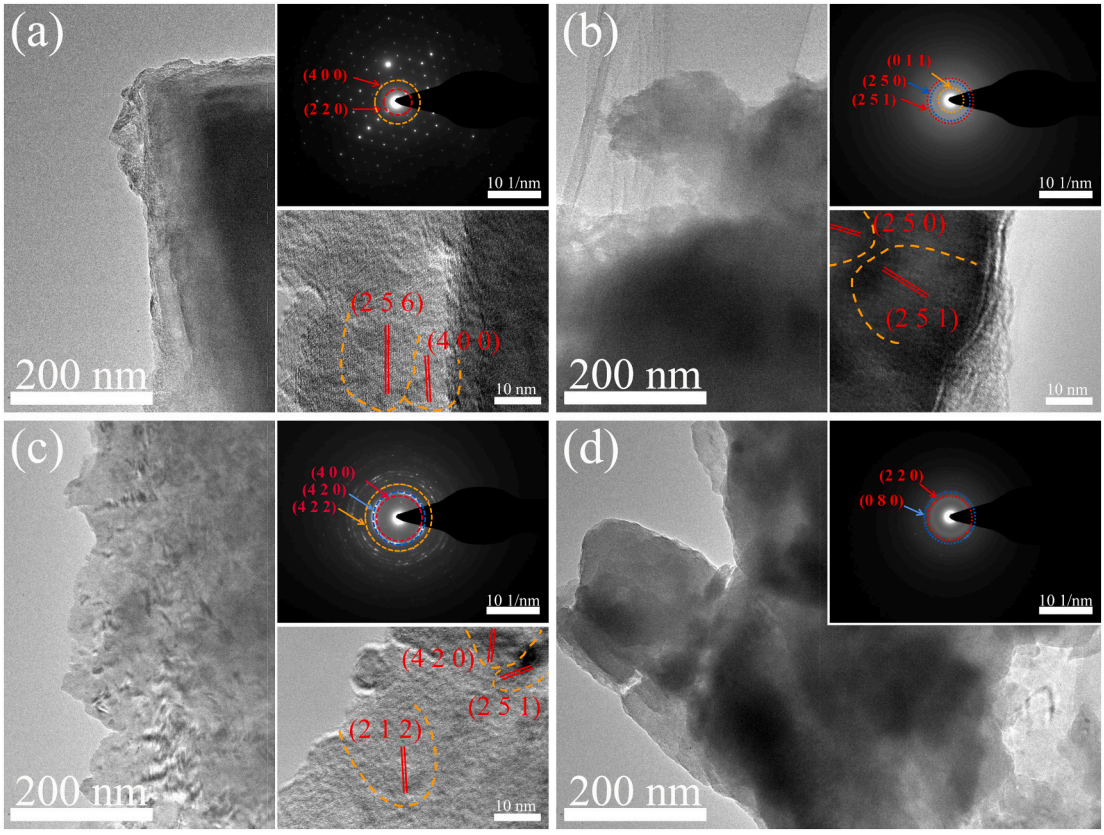

Fig. 6. HRTEM images and the selected area electron diffraction (SAED) patterns of the GCPCC coating obtained at 50 °C for 30 min. (a) UD Ti/Fe-F, (b) CD Ti/Fe-F, (C) UD Ti/Fe-L, (D) CD Ti/Fe-L.

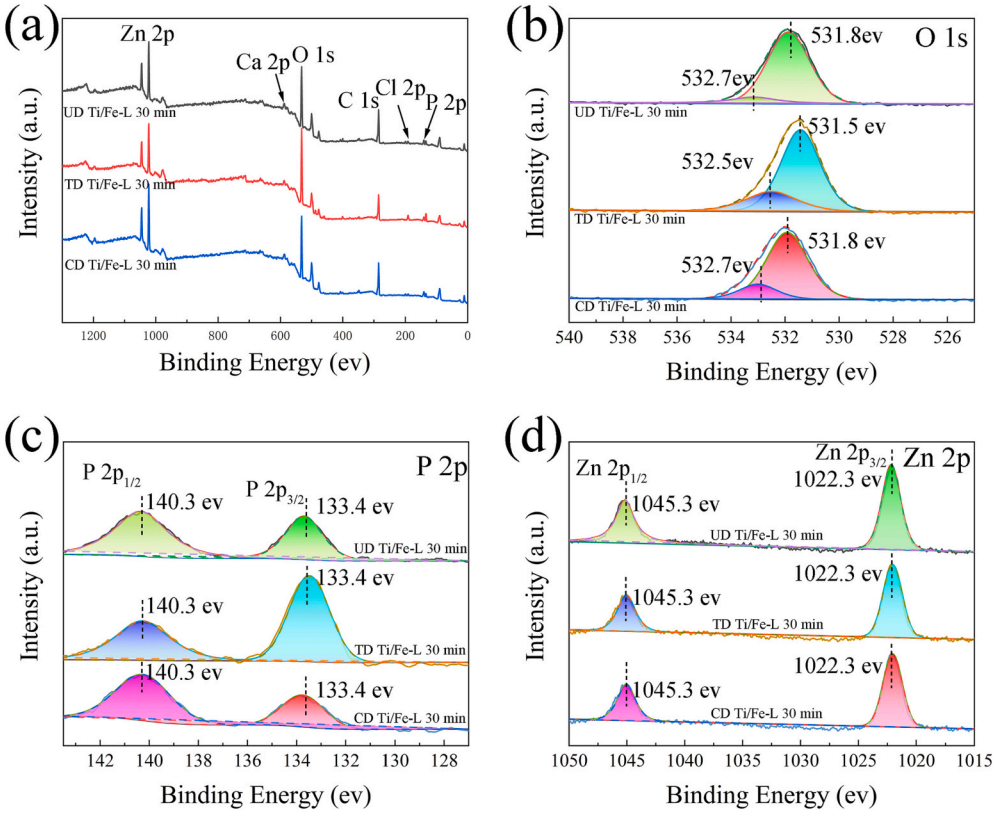

Fig. 7. The typical XPS spectra of the GCPCC samples treated by Ti/Fe-L. (a) survey scanning spectra, and high-resolution spectra of (b) O 1s, (c) P 2p, and (d) Zn 2p, respectively.

Studies have shown that all elements necessary for the formation of insoluble phosphates adhere to metal surfaces in an amorphous state before undergoing crystallization. This observation further shows that the compression deformation of TC4 is not conducive to the crystallization of hopeite under the same conversion timeframe.

Fig. 4 shows the FTIR spectra of the conversion coatings formed by chemical conversion under two different contact modes. In both spectra, typical absorption peaks for PO_4^{3+} and OH^- groups further verify the hopeite phase measured in the XRD in Fig. 3. The absorption peak at 1018 cm^{-1} is the asymmetric stretching vibration absorption peak of PO_4^{3+}, the strong absorption band at 939 cm^{-1} is the symmetric stretching vibration absorption peak of P═O, and the absorption peaks at 576 cm^{-1} and 631 cm^{-1} are bending vibration peaks of O = P = O bonds [38].

The EDS mapping diagrams of the chemical conversion coating under the action of multipoint coupling and line coupling are presented in Fig. 5. In addition to the Ti, Al, and V elements of the TC4 substrate, the main components of the conversion coating are Zn, P, and O. Combining the XRD (Fig. 3) and FTIR (Fig. 4) results, it is firmly established that the main components of the conversion coating are hopeite and amorphous ZnP granular coatings.

As depicted in Fig. 5, the morphology of the multipoint coupled conversion coating is similar to that of the amorphous coating, and the crystal morphology features are less distinct than those of the line-coupled conversion coating. This observation indicates that multipoint coupling may not be suitable for the formation of hopeite at 50 °C. Upon further analysis, in conjunction with Fig. 1 and Fig. 3, when the temperature is increased to 70 °C, the advantages of multipoint coupling are fully exploited in comparison with line coupling. Under the multipoint coupling mode, fine and uniform hopeite crystals can be formed. In addition, the presence of Fe elements in the EDS of the conversion coating formed in the multipoint coupling mode is the multipoint Fe formed on the TC4 surface after the magnetron sputtering treatment.

Fig. 6 shows the HRTEM images and selected area electron diffraction of the chemical conversion coating under the action of multipoint coupling and line coupling. The lattice fringes displayed in different regions of HRTEM correspond to crystal planes such as (400), (251) and (420). This correspondence implies that the conversion coatings in several cases all contain hopeite. From the lattice fringes and electron diffraction patterns in Fig. 6(a) and (c), it becomes apparent that the surface conversion coating of the unplastically deformed TC4 exhibits obvious hopeite crystal characteristics under both coupling modes, indicating that the crystallinity of the GCPCC coating on the unplastic deformed sample has good crystallinity.

The selected area diffraction patterns in Fig. 6(b) and (d) exhibit diffuse circular rings, which are characteristic of amorphous materials. Meanwhile, there are a few bright spots scattered around the diffuse rings, suggesting that the products are mostly amorphous and accompanied by a few grain characteristics. This indicates that the chemical transformation of TC4 after compression promotes the formation of amorphous crystals but is not conducive to the formation of crystals. These findings align with the results obtained from XRD in Fig. 3.

To accurately analyse the compounds formed by various elements and to further characterize their chemical composition, XPS detection was performed on the coating. According to the full XPS spectra in Fig. 7 (a) and Fig. 8 (a), the elements contained in the conversion coating include P, O, Zn, C, and Ca. Due to the inevitable exposure of the sample to air after conversion, C was detected by XPS. The binding energy of other elements is calibrated using a C 1 s peak with a binding energy of 284.8 eV. It can be seen from the XPS full spectrum that the conversion coating contains Ca with a low intensity peak, which proves that calcium ions also participate in the formation of the coating [39]. However, no diffraction peak of calcium compounds was found in the XRD phase analysis, which can be attributed to the relatively low content of $Zn_2Ca(PO_4)_2{\cdot}4H_2O$ in the conversion coating and cannot be detected by XRD.

For the O 1 s spectrum (Fig. 7(b)), the main peaks located at 531.8 eV

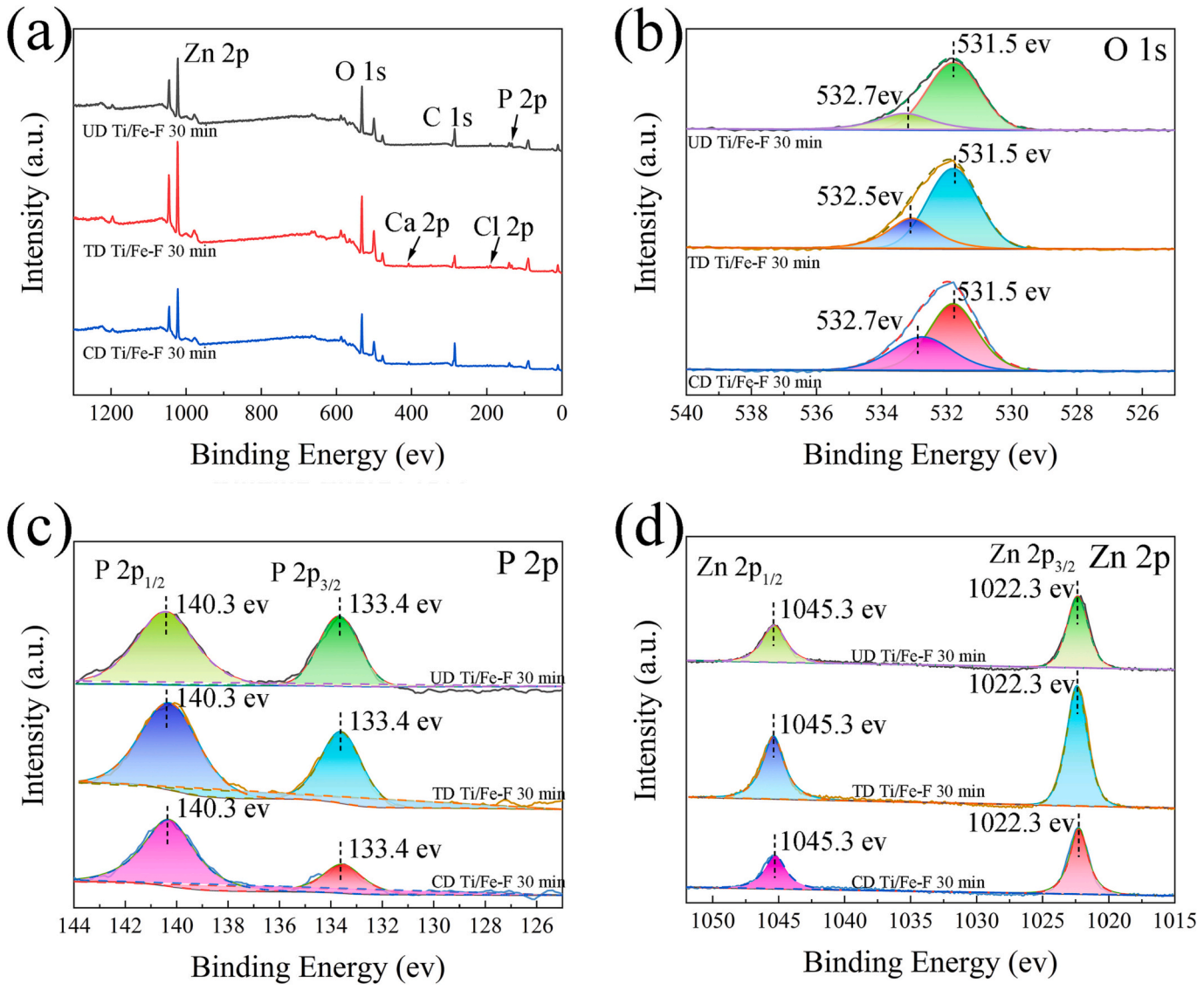

Fig. 8. The typical XPS spectra of the GCPCC samples treated by Ti/Fe-F. (a) survey scanning spectra, and high-resolution spectra of (b) O 1s, (c) P 2p, and (d) Zn 2p, respectively.

and 531.5 eV are assigned to PO_4^{3-} in hopeite. Given the presence of Ca in the full spectrum, the peak of O 1 s at 532.7 eV should be attributed to the phosphide of calcium. Figs. 7(c) and 8(c) show the narrow scan spectra of P 2p, indicating that the P 2p element exhibits a spin orbit splitting double peak. The binding energies of P 2p at 133.4 eV and 140.3 eV correspond to P $2p_{3/2}$ and P $2p_{1/2}$, respectively, which are ascribed to PO_4^{3-}. The high-resolution spectrum of Zn 2p is also divided into two peaks, and the peaks at 1045.3 eV and 1022.3 eV belong to Zn $2p_{3/2}$ and Zn $2p_{1/2}$, respectively [40]. The above XPS results further confirm that the main component of the conversion film is hopeite.

3.2. Coating properties

Fig. 9 and Fig. 10 show the potentiodynamic polarization curves and EIS diagrams of the chemical conversion coating under the action of multipoint coupling and line coupling at 50 °C. Table 2 and Table 3 are the results of the self-corrosion potential (E_{corr}) and corrosion current density (I_{corr}) calculated from the polarization curves according to the Tafel extrapolation method. Overall, the E_{corr} of the conversion coating formed by the line coupling contact method exceeds that of the conversion coating formed by the multipoint coupling method, while the I_{corr} of the conversion coating formed by the line coupling contact method is lower than that of the conversion coating formed by the multipoint coupling method. This indicates that the corrosion resistance of the conversion coating formed by line coupling at 50 °C is higher than that formed by multipoint coupling. Based on the morphological and structural characterization, it is apparent that the conversion coating formed by the multipoint coupling method has more amorphous phases and less hopeite at 50 °C. This implies that hopeite has an excellent effect on improving the corrosion resistance of TC4. Compared with the line coupling mode, the hopeite coating formed by multipoint coupling is denser and has fine particles at 70 °C. It is further speculated that the corrosion resistance of the conversion coating formed by multipoint coupling at high temperature should be better.

EIS is a commonly employed method for characterizing the electrochemical corrosion behaviour of coatings. In Fig. 9(b) and Fig. 10(b), the Nyquist plots show that the Nyquist point of all the conversion coatings exhibits an incomplete semicircular arc with a larger radius, indicating that the corrosion behaviour of the conversion coating is similar in 0.9 % NaCl and has a high polarization resistance and good corrosion resistance.

Fig. 9(c) and Fig. 10(c) show the impedance value |Z| as a function of

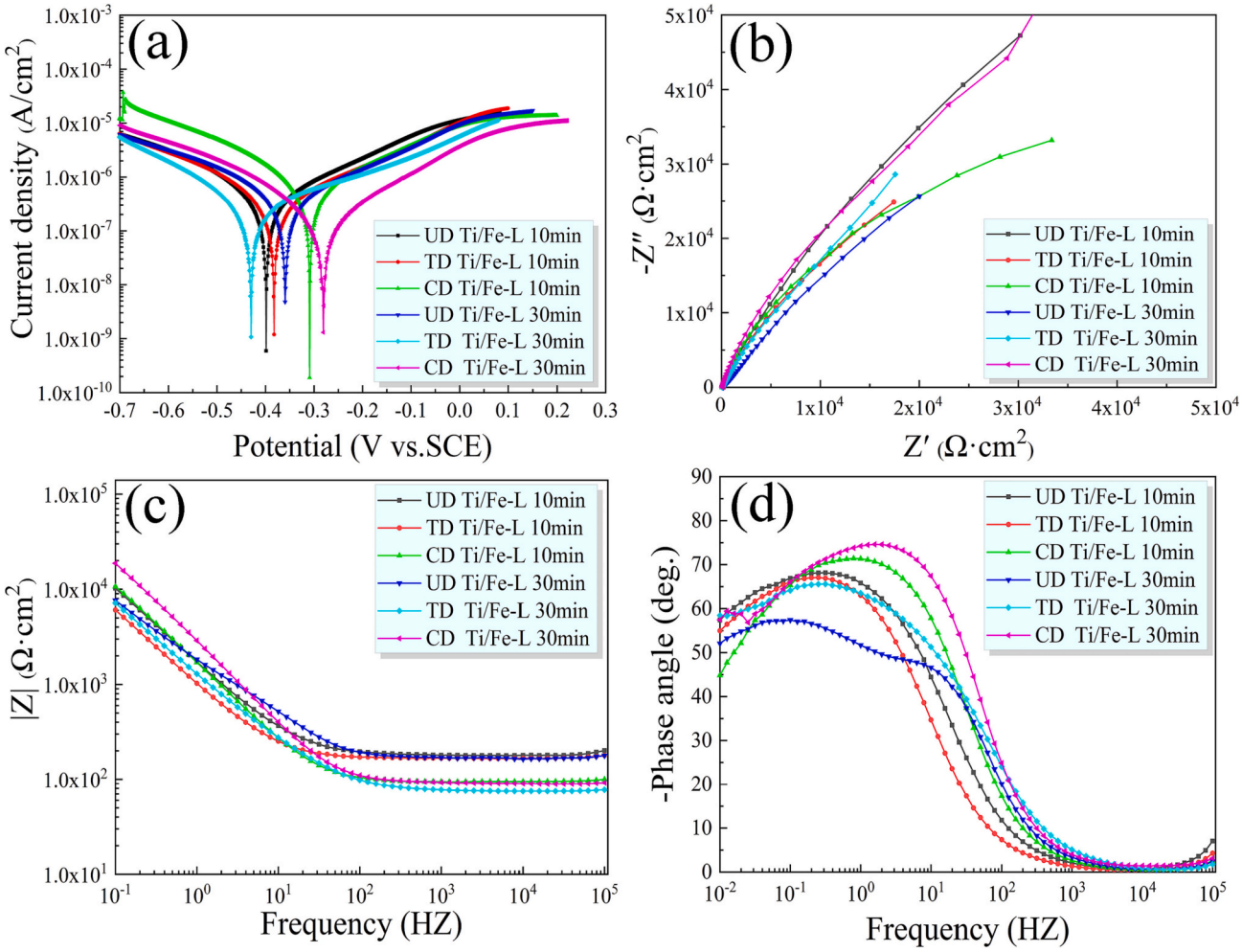

Fig. 9. Potentiodynamic polarization curves (a) and Electrochemical impedance diagrams (b)-(d) of the GCPCC samples treated by Ti/Fe-L.

the disturbance frequency in the Bode diagram. When the impedance value is high, the corrosion resistance of the sample will be enhanced. In the low-frequency region, most of the conversion coating samples in the line-coupling mode have higher impedance values than those formed by multipoint coupling. This observation aligns with the results of the previous Tafel analyses.

The fitted parameters obtained from the EIS results are detailed in Table 4. R_s represents the electrolyte resistance, R_c is the coating resistance, R_{ct} is the charge transfer resistance. To address the non-ideal capacitance resulting from the uneven surface of the sample coating, Q was employed as a substitute for the pure capacitor C. Q_c is the coating capacitance, and Q_{dl} is the double layer capacitance. Upon scrutiny of the $R_c + R_{ct}$ values, it becomes apparent that the line coupling at 50 °C surpasses that of the multipoint coupling. Based on the findings, the corrosion resistance of the sample improves with a greater impedance $R_c + R_{ct}$. This conclusion aligns with the findings presented in Tables 2 and 3.

Fig. 11 illustrates the variation in the friction coefficient with sliding time for different samples under 2 N and 5 N loads. In general, the majority of samples exhibit a lower friction coefficient at 2 N than at 5 N. In addition, under the same experimental conditions, the compressed sample displays the lowest friction coefficient. On the one hand, this result can be attributed to the fact that, in addition to a small amount of hopeite, the composition of the conversion coating on the surface of the compressed sample also contains a quasiamorphous ZnP granular coating. On the other hand, because the compression treatment changes the TC4 substrate structure, it will also affect the friction performance to a certain extent.

Fig. 12 demonstrates the average friction coefficient and wear amount of the samples under different treatment conditions. A comparison of the wear loss of the samples reveals that the wear loss of 5 N was significantly greater than that of 2 N. This discrepancy is primarily due to the higher the load, the greater the degree of bite between the friction contact surfaces, the plastic shear effect is enhanced, and the wear degree of the friction surface also increases. In addition, the wear loss of the conversion coating formed on the compressed sample is minimal for either 2 N or 5 N loading, and the coating has the least resistance to wear under this condition, both because of the granular structural characteristics of the conversion coating on the compressed sample and the influence of the structure of the sample substrate after compression.

3.3. Phosphate growth mechanism

Due to the presence of a stable oxide passivation layer on the surface of Ti and its alloys, conventional chemical conversion methods are insufficient to form a conversion coating on their surface. In this study, the principle of galvanic coupling was utilized to facilitate the chemical transformation of TC4 surfaces. Galvanic coupling, a type of galvanic corrosion, refers to the phenomenon of bimetallic corrosion occurring when metals with different electrode potentials come into contact and are in a conductive solution medium. Iron (Fe) with a lower corrosion potential was selected as the coupling anode, and TC4 with a higher corrosion potential was used as the coupling cathode. The initial driving

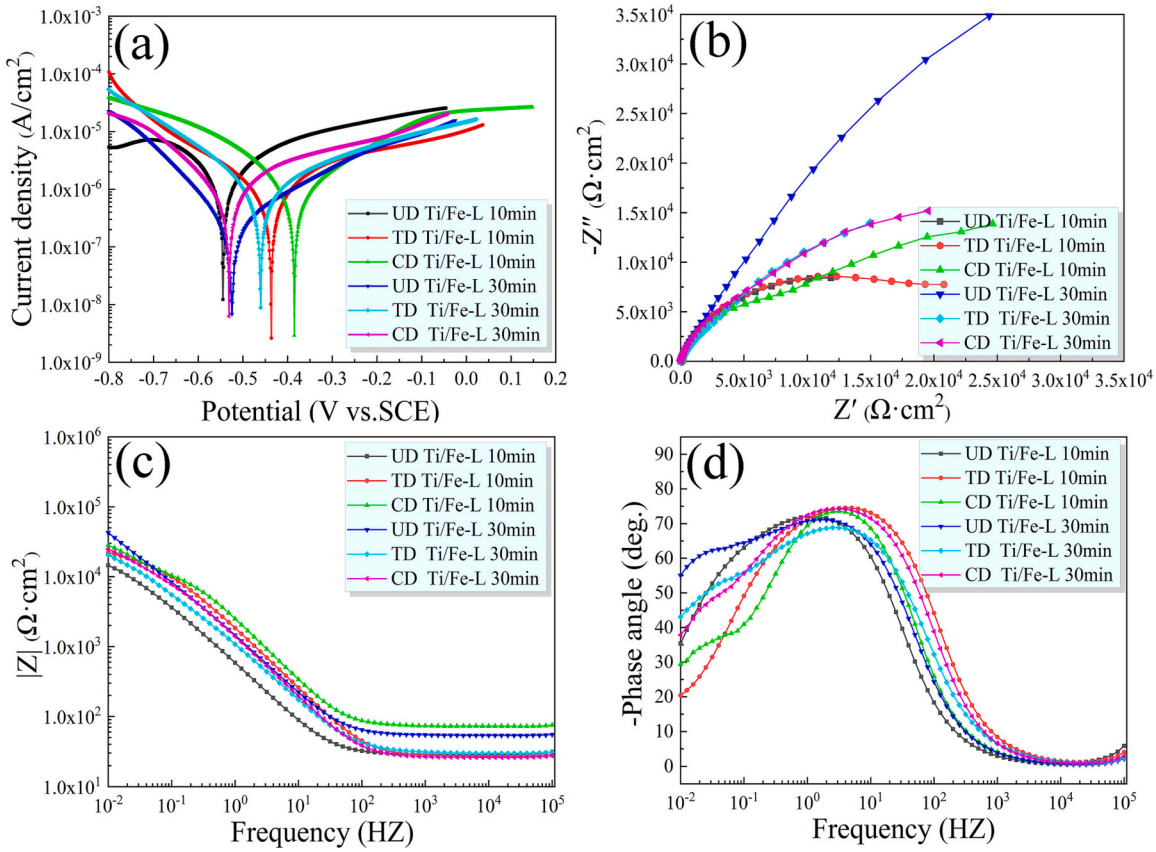

Fig. 10. Potentiodynamic polarization curves (a) and Electrochemical impedance diagrams (b)-(d) of the GCPCC samples treated by Ti/Fe-F.

Table 2
The self-corrosion potential and self-corrosion current of Ti/Fe-L samples.

Samples	UD Ti/Fe-L 10 min	TD Ti/Fe-L 10 min	CD Ti/Fe-L 10 min	UD Ti/Fe-L 30 min	TD Ti/Fe-L 30 min	CD Ti/Fe-L 30 min
E_{corr} (mv, SCE)	−396	−376	−310	−355	−428	−280
I_{corr} (μA/cm^2)	0.2586	0.2305	0.4200	0.2198	0.1848	0.1069

Table 3
The self-corrosion potential and self-corrosion current of Ti/Fe-F samples.

Samples	UD Ti/Fe-F 10 min	TD Ti/Fe-F 10 min	CD Ti/Fe-F 10 min	UD Ti/Fe-F 30 min	TD Ti/Fe-F 30 min	CD Ti/Fe-F 30 min
E_{corr} (mv, SCE)	−540	−436	−381	−524	−460	−541
I_{corr} (μA/cm^2)	1.5391	0.6419	0.7393	0.2208	0.6744	0.7269

force for the chemical transformation of the metal surface is generated by the potential difference between the cathode and the anode in the coupled system. The greater the potential difference is, the greater the initial driving force.

Fe^{2+} dissolution occurs on the surface of the coupled anode Fe in the anode region, as shown in reaction (1). The hydrogen evolution reaction occurs on the surface of the coupled cathode TC4 as the cathode region, as shown in reaction (2). During this hydrogen evolution reaction, free phosphoric acid in the solution is rapidly consumed, leading to an increase in the pH value of the metal-solution interface [41], and the local pH value will be significantly higher than the macroscopic measurement of the conversion solution. As the conversion solution is a phosphate buffer solution, minor fluctuations in pH can result in a significant variation in the concentration of $H_2PO_4^-/HPO_4^{2-}$ [42]. Under chemical equilibrium, the phosphoric acid in the solution undergoes further ionization, as shown in reaction (3).

$$Fe - 2e^- \rightarrow Fe^{2+} \quad (1)$$

Table 4
Fitted parameters of the EIS results.

	R_s (Ω·cm^2)	Q_c (μF·cm^{-2})	n_c	R_c (KΩ·cm^2)	Q_{dl} (μF·cm^{-2})	n_{dl}	R_{ct} (KΩ·cm^2)
UD Ti/Fe-L 30 min	167.7	44.87	0.9	0.9098	149	0.6455	214
TD Ti/Fe-L 30 min	75.16	91.71	0.8463	0.2547	111.9	0.6659	216.3
CD Ti/Fe-L 30 min	90.58	68.24	0.8835	76.67	41.64	0.8761	228.2
UD Ti/Fe-F 30 min	53.54	130.3	0.8	9.539	75.55	0.8	194
TD Ti/Fe-F 30 min	29.93	180.1	0.8481	5.361	136	0.5499	63.43
CD Ti/Fe-F 30 min	26.02	130.3	0.8929	7.718	127	0.4678	52.72

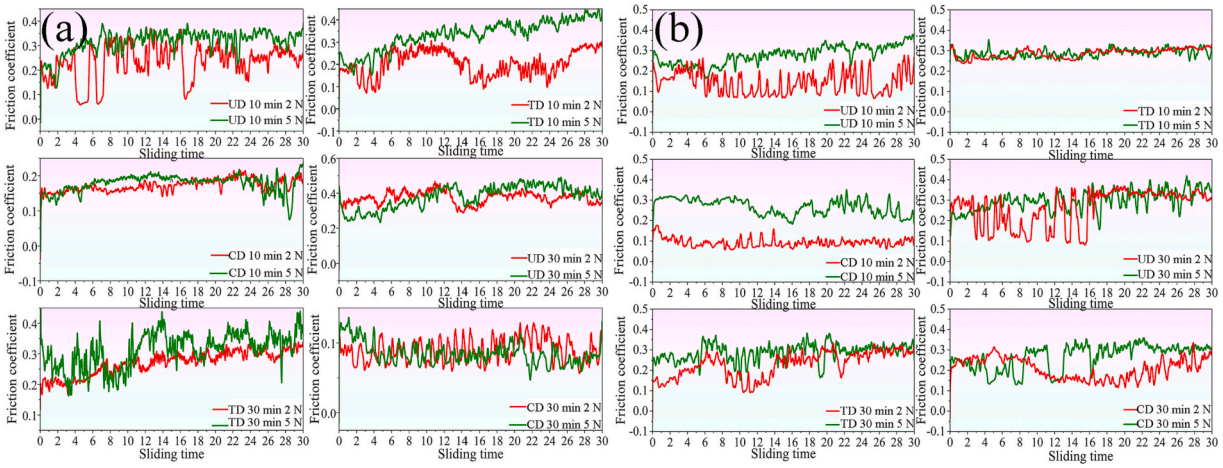

Fig. 11. Friction coefficient curves of the conversion coatings formed under different coupling modes at 2 N and 5 N loads. (a) Ti/Fe-L, (b) Ti/Fe-F.

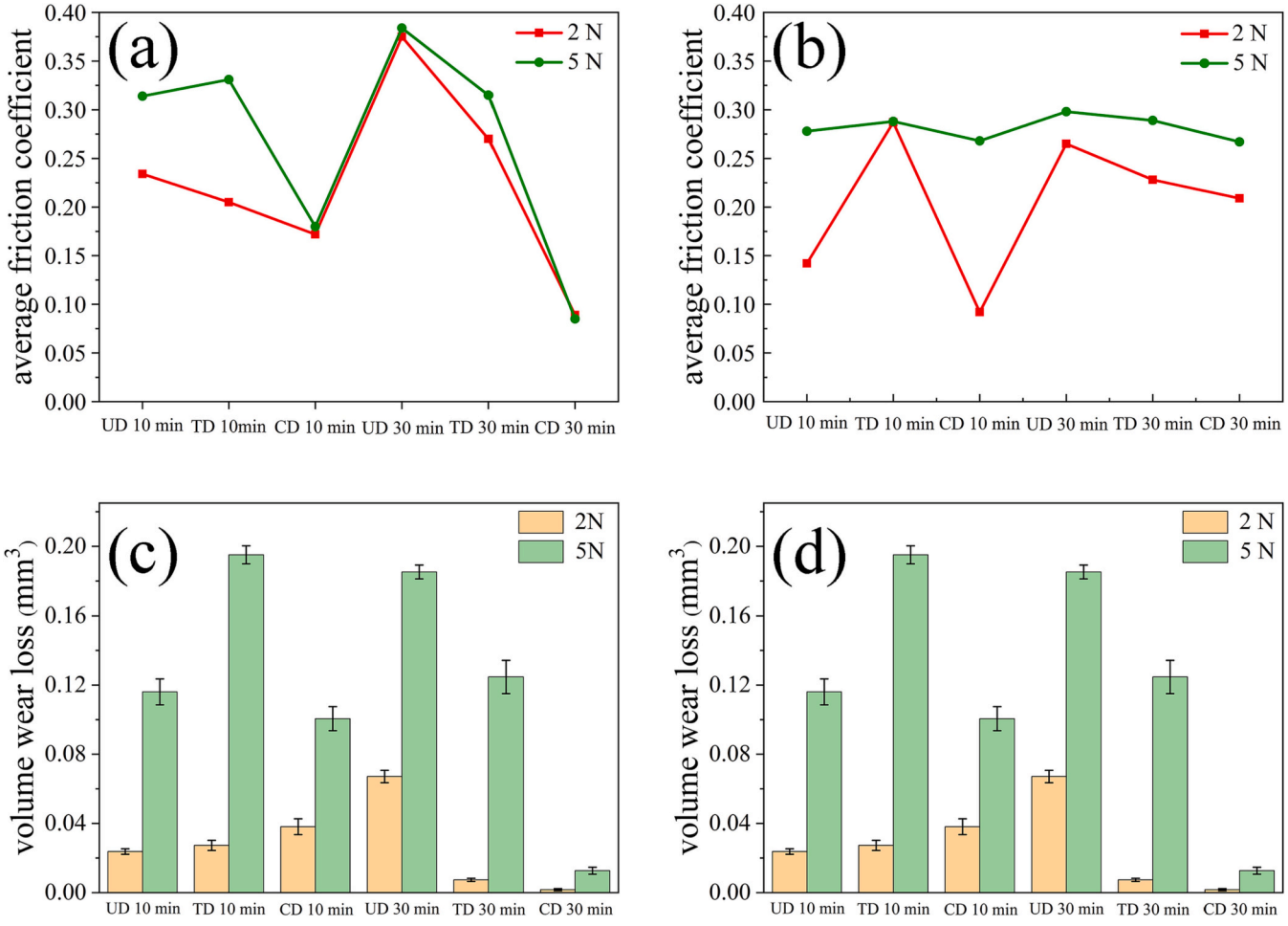

Fig. 12. Average friction coefficient of (a) Ti/Fe-L and (b) Ti/Fe-F. Wear rate of (c) Ti/Fe-L and (d) Ti/Fe-F.

$$2H^+ + 2e^- \rightarrow H_2\uparrow \quad (2)$$

$$H_3PO_4 \rightarrow H_2PO_4^- + H^+ \rightarrow HPO_4^{2-} + 2H^+ \rightarrow PO_4^{3-} + 3H^+ \quad (3)$$

$$3Zn^{2+} + 2PO_4^{3-} + 4H_2O \rightarrow Zn_3(PO_4)_2 \cdot 4H_2O\downarrow \quad (4)$$

The above reaction occurs in the presence of more PO_4^{3-} at the metal-solution interface. Zn^{2+} and PO_4^{3-} in the solution will reach a supersaturated state on the metal surface due to the increased pH, leading to crystallization and nucleation on the surface of TC4. The main chemical reactions occurring at this stage can be summarized as shown in reaction (4). Prior to crystallization, an amorphous precipitation coating is generated on the metal surface [37].

Fig. 13 shows the chemical conversion mechanism of line coupling and multipoint coupling. In this study, two galvanic coupling methods, linear coupling and multipoint coupling, were employed. At 70 °C, when

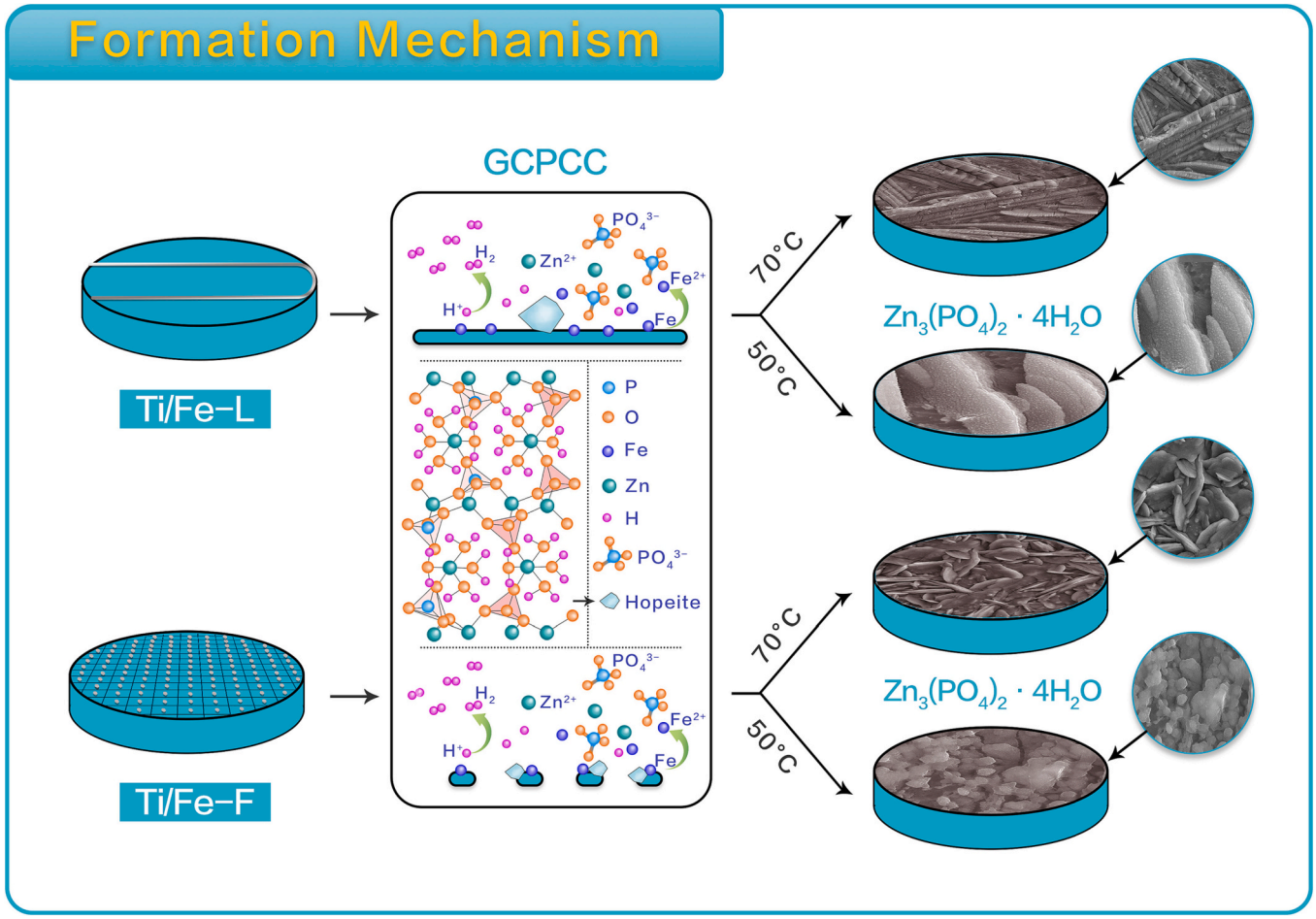

Fig. 13. Schematic diagram of the formation mechanism of the GCPCC coatings treated by Ti/Fe-L and Ti/Fe-F.

multipoint coupling is utilized as the coupling anode, it results in a finer and more uniform chemical conversion coating compared to line coupling. The reason for the small size of the conversion coating is that the changes in crystal structure and morphology are related to the formation rate of the conversion coating, which in turn depends on the number of nucleation sites on the surface of the TC4 substrate. Multipoint coupling makes the Fe used as the coupling anode evenly distributed on the surface of TC4 in a grid-like manner. As a result, there are many more hopeite nucleation sites on the surface of the TC4 substrate than on the line coupling. In contrast, the number of initial nucleation crystals formed on the surface of the line-coupled TC4 substrate is less, which makes the conversion coating formation rate slower and the coating formation induction period longer. The crystal epitaxial growth will be obvious, leading to a larger crystal size in the formed coating.

As the generation rate of the multipoint coupling conversion coating increases, that is, the coating formation induction period is shortened, the number of 'active centres' on the surface of the substrate increases, the number of initial crystal nucleations is large, and the crystal growth space is restricted, so the size of the formed crystals will be smaller. This is the main reason for the fine grain size of the multipoint coupling conversion coating.

In addition, the galvanic corrosion rate is related to the area ratio of the cathode and anode phases [43,44]. In an acidic conversion solution, the multipoint coupled Fe simultaneously undergoes uniform corrosion at multiple locations on the surface of TC4, resulting in a consistent overall pH value on the surface of TC4, and thus, the nucleation and growth of the conversion coating are basically uniform. This is the main reason for the uniform coating of the multipoint coupling conversion coating.

Temperature is also a crucial factor affecting chemical conversion [45]. In this study, compared to the hopeite conversion coating formed at 70 °C that completely covers the TC4 substrate, the amount of hopeite in the conversion coating formed at 50 °C is relatively lower. In particular, hopeite cannot be easily observed when multipoint coupling occurs because chemical conversion is an endothermic process. Generally, higher temperatures favour the conversion process [36].

At lower chemical temperatures, the substrate surface is in a state of waiting to be excited due to the insufficient energy needed for the crystalline core. Therefore, the formation rate of the conversion coating is low, resulting in a decrease in the number of crystals and coarsening of individual grains. In the case of multipoint coupling at lower temperatures, initiating the conversion process becomes more challenging. Hence, the coating exists more in an amorphous form. Additionally, during the conversion process, the plastic deformation of the TC4 substrate also affects the morphology of the conversion coating. Especially when the substrate is in a compressed state, the organizational structure in the conversion coating changes. This is because changes in the substrate structure affect the nucleation sites and energy states of the conversion substrate.

4. Conclusions

In this study, the principle of galvanic coupling was utilized to facilitate the chemical transformation of the TC4 surface. Fe, known for its low corrosion potential, was chosen as the coupling anode, and TC4, characterized by high corrosion potential, served as the coupling cathode. The initial driving force for chemical transformation on the metal

surface was established through the potential difference between the cathode and anode in the coupling system. Two galvanic coupling methods, line coupling and multipoint coupling, were employed. At 70 °C, when utilizing multipoint coupling as the coupling anode, the chemical conversion coating formed on the surface of the coupling cathode TC4 was finer and more uniform in comparison to line coupling. Multipoint coupling evenly distributes Fe as the coupling anode on the surface of TC4 in a grid-like manner, resulting in a significantly larger number of hopeite nucleation sites on the TC4 surface compared to line coupling. The number of crystals initially nucleated was large, and the crystal growth space was suppressed, so the size of the formed crystals was relatively small and uniform. Elevated temperature changed the composition and integrity of the coating. At 50 °C, the coatings obtained by the chemical conversion treatment were hopeite and amorphous ZnP-like granular coatings, while the chemical conversion coatings were predominantly hopeite at 70 °C. The plastic deformation of the TC4 substrate also affects the morphology of the conversion coating.

CRediT authorship contribution statement

YaJun Li: Data curation, Investigation, Writing – original draft. **Wenhua Xu:** Conceptualization, Data curation. **Ningbo Li:** Formal analysis, Methodology. **Zhen Ma:** Investigation. **Baoxu Huang:** Writing – review & editing. **Jie Ma:** Data curation, Writing – review & editing. **Hui Chen:** Data curation, Resources. **Xuehui Hao:** Writing – review & editing. **Xingchuan Zhao:** Conceptualization, Funding acquisition, Methodology, Supervision, Writing – review & editing.

Declaration of competing interest

We declare that we have no conflict of interest.

Data availability

Data will be made available on request.

Acknowledgements

The work was supported by Natural Science Foundation of Shandong Province (Grant No.ZR2021ME083).

References

[1] X. Han, J. Ma, A. Tian, Y. Wang, Y. Li, B. Dong, X. Tong, X. Ma, Surface modification techniques of titanium and titanium alloys for biomedical orthopaedics applications: a review, Colloids Surf. B: Biointerfaces 227 (2023) 113339.
[2] Z. Wang, L. Mei, X. Liu, Q. Zhou, Hierarchically hybrid biocoatings on Ti implants for enhanced antibacterial activity and osteogenesis, Colloids Surf. B: Biointerfaces 204 (2021) 111802.
[3] L. Guo, S. Ataollah Naghavi, Z. Wang, S. Nath Varma, Z. Han, Z. Yao, L. Wang, L. Wang, C. Liu, On the design evolution of hip implants: a review, Mater. Des. 216 (2022) 110552.
[4] E. Ranjit, S. Hamlet, R.M. Love, Keratin coated titanium as an aid to osseointegration: physicochemical and mechanical properties, Surf. Coat. Technol. 462 (2023) 129457.
[5] M. Kaur, K. Singh, Review on titanium and titanium based alloys as biomaterials for orthopaedic applications, Mater. Sci. Eng. C 102 (2019) 844–862.
[6] M. Mansoorianfar, A. Khataee, Z. Riahi, K. Shahin, M. Asadnia, A. Razmjou, A. Hojjati-Najafabadi, C. Mei, Y. Orooji, D. Li, Scalable fabrication of tunable titanium nanotubes via sonoelectrochemical process for biomedical applications, Ultrason. Sonochem. 64 (2020) 104783.
[7] C. Alizade, A. Jafarov, G. Berchenko, O.S. Bicer, F. Alizada, Investigation of the process intergrowth of bone tissue into the hole in titanium implants (experimental research), Injury 53 (2022) 2741–2748.
[8] W. Yang, X. Liu, Y. Fang, S. Attarilar, C. Zhu, L. Wang, Q. Luo, Y. Fu, Osteogenic differentiation of bone marrow stromal stem cells on a novel β titanium alloy-based micro-nano composite, J. Mater. Res. Technol. 24 (2023) 5864–5875.
[9] L. Shanmuganantha, M.U. Aslam Khan, A.B. Sulong, M.I. Ramli, A. Baharudin, H. M. Ariffin, S.I. Abd Razak, M.H. Ng, Characterization of titanium ceramic composite for bone implants applications, Ceram. Int. 48 (2022) 22808–22819.
[10] Y. Ding, B. Tao, R. Ma, X. Zhao, P. Liu, K. Cai, Surface modification of titanium implant for repairing/improving microenvironment of bone injury and promoting osseointegration, J. Mater. Sci. Technol. 143 (2023) 1–11.
[11] P. Jiang, Y. Zhang, R. Hu, B. Shi, L. Zhang, Q. Huang, Y. Yang, P. Tang, C. Lin, Advanced surface engineering of titanium materials for biomedical applications: from static modification to dynamic responsive regulation, Bioact. Mater. 27 (2023) 15–57.
[12] L. Liu, F. Ma, B. Kang, P. Liu, S. Qi, W. Li, K. Zhang, X. Chen, Preparation and mechanical and biological performance of the Sr-containing microarc oxidation layer on titanium implants, Surf. Coat. Technol. 463 (2023) 129530.
[13] L. Sousa, R.D.M. Antunes, J.C.S. Fernandes, A.C. Alves, F. Toptan, Influence of Al_2O_3 reinforcements and Ti-Al intermetallics on corrosion and tribocorrosion behavior of titanium, Surf. Coat. Technol. 470 (2023) 129835.
[14] M. Geetha, A.K. Singh, R. Asokamani, A.K. Gogia, Ti based biomaterials, the ultimate choice for orthopaedic implants – a review, Prog. Mater. Sci. 54 (2009) 397–425.
[15] N. Jambhulkar, S. Jaju, A. Raut, B. Bhoneja, A review on surface modification of dental implants among various implant materials, Mater. Today Proc. 72 (2023) 3209–3215.
[16] A. Kurup, P. Dhatrak, N. Khasnis, Surface modification techniques of titanium and titanium alloys for biomedical dental applications: a review, Mater. Today Proc. 39 (2021) 84–90.
[17] L. Herschke, J. Rottstegge, I. Lieberwirth, G. Wegner, Zinc phosphate as versatile material for potential biomedical applications Part 1, J. Mater. Sci. Mater. Med. 17 (2006) 81–94.
[18] S.M.A. Shibli, A.C. Jayalekshmi, Development of phosphate inter layered hydroxyapatite coating for stainless steel implants, Appl. Surf. Sci. 254 (2008) 4103–4110.
[19] X.K. Shen, Y. Hu, G.Q. Xu, W.Z. Chen, K. Xu, Q.C. Ran, P.P. Ma, Y.R. Zhang, J.H. Li, K.Y. Cai, Regulation of the biological functions of osteoblasts and bone formation by zn-incorporated coating on microrough titanium, ACS Appl. Mater. Interfaces 6 (2014) 16426–16440.
[20] Q.M. Zhao, G.H. Xu, A.N. Hu, R.S. Xu, H.R.C. Jin, Y.Y. Sun, G.F. Bao, K. Yuan, X. G. Zhou, X. Wang, Z.M. Cui, A Mg/Zn-co-doped composite coating on a titanium surface enhances osteogenic activity through the Wnt/β-catenin pathway, Appl. Surf. Sci. 515 (2020) 146072.
[21] Y. Wang, S. Zhao, G. Li, S. Zhang, R. Zhao, A. Dong, R. Zhang, Preparation and in vitro antibacterial properties of anodic coatings co-doped with Cu, Zn, and P on a Ti-6Al-4V alloy, Mater. Chem. Phys. 241 (2020) 122360.
[22] S. Durdu, A. Arslanturk, S.L. Aktug, K. Korkmaz, S. Aktas, F. Unal, E. Yalcin, K. Cavusoglu, A comparison study on bioactivity and antibacterial properties of Ag-, Cu- and Zn-deposited oxide coatings produced on titanium, J. Mater. Sci. 57 (2022) 17203–17218.
[23] Q. Bi, X. Song, Y. Chen, Y. Zheng, P. Yin, T. Lei, Zn-HA/Bi-HA biphasic coatings on titanium: fabrication, characterization, antibacterial and biological activity, Colloids Surf. B: Biointerfaces 189 (2020) 110813.
[24] O. Lunder, J.C. Walmsley, P. Mack, K. Nisancioglu, Formation and characterisation of a chromate conversion coating on AA6060 aluminium, Corros. Sci. 47 (2005) 1604–1624.
[25] N. Banjo, T.T. Sasaki, K. Hono, Microstructure control of Ti-based conversion coatings for optimizing organic coating properties in A6063 and A3003 alloys, Surf. Coat. Technol. 468 (2023) 129735.
[26] S. Silva-Fernández, B. Díaz, I. Feijoo, X.R. Nóvoa, C. Pérez, Influence of pH and temperature in the performance of Zn phosphate conversion coatings, Electrochim. Acta 457 (2023) 142510.
[27] N. Van Phuong, S. Moon, Comparative corrosion study of zinc phosphate and magnesium phosphate conversion coatings on AZ31 Mg alloy, Mater. Lett. 122 (2014) 341–344.
[28] A.H. Riyas, C.V. Geethanjali, S. Arathy, A. Anil, S.M.A. Shibli, Exploration and tuning of Al_2O_3/Mo composite for enhancement of anti-corrosion and tribological characteristics in zinc phosphate conversion coatings, Appl. Surf. Sci. 593 (2022) 153370.
[29] B. Liu, X. Zhang, G.Y. Xiao, Y.P. Lu, Phosphate chemical conversion coatings on metallic substrates for biomedical application: a review, Mater. Sci. Eng. C 47 (2015) 97–104.
[30] H.Y. Su, C.S. Lin, Effect of additives on the properties of phosphate conversion coating on electrogalvanized steel sheet, Corros. Sci. 83 (2014) 137–146.
[31] A. Valanezhad, K. Tsuru, M. Maruta, G. Kawachi, S. Matsuya, K. Ishikawa, Zinc phosphate coating on 316L-type stainless steel using hydrothermal treatment, Surf. Coat. Technol. 205 (2010) 2538–2541.
[32] A. Valanezhad, K. Tsuru, M. Maruta, G. Kawachi, S. Matsuya, K. Ishikawa, A new biocompatible coating layer applied on titanium substrates using a modified zinc phosphatizing method, Surf. Coat. Technol. 206 (2012) 2207–2212.
[33] B. Liu, G.Y. Xiao, C.C. Jiang, Y.Z. Zheng, L.L. Wang, Y.P. Lu, Formation initiation and structural changes of phosphate conversion coating on titanium induced by galvanic coupling and Fe^{2+} ions, RSC Adv. 6 (2016) 75365–75375.
[34] P. Zhou, H. Guo, M. Li, C. Zhang, B. Yu, Y. Zhai, Y. Chen, J. Sun, Y. Yuan, T. Zhang, F. Wang, Preheating Mg alloy before the phosphate conversion treatment: the enhanced crystal precipitation kinetics associated with the elevated temperature at reaction fronts, Electrochim. Acta 431 (2022) 141153.
[35] K.J. Laidler, The development of the Arrhenius equation, J. Chem. Educ. 61 (1984) 494.
[36] M. Fouladi, A. Amadeh, Effect of phosphating time and temperature on microstructure and corrosion behavior of magnesium phosphate coating, Electrochim. Acta 106 (2013) 1–12.

[37] T. Sankara Narayanan, Surface pretretament by phosphate conversion coatings-a review, Rev. Adv. Mater. Sci. 9 (2005) 130–177.
[38] K.S. Fernandes, E.D.A. Alvarenga, P.R.G. Brandao, V.D.F.C. Lins, Infrared-spectroscopy analysis of zinc phosphate and nickel and manganese modified zinc phosphate coatings on electrogalvanized steel, Rem: Revista Escola de Minas 64 (2011) 45–49.
[39] U.B. Nair, Calcium as a phosphating additive: an overview, Met. Finish. 93 (1995) 40–41.
[40] B. Liu, G.Y. Xiao, Y.P. Lu, Effect of pH on the phase composition and corrosion characteristics of calcium zinc phosphate conversion coatings on titanium, J. Electrochem. Soc. 163 (2016) C477–C485.
[41] G. Duan, L. Yang, S. Liao, C. Zhang, X. Lu, Y. Yang, B. Zhang, Y. Wei, T. Zhang, B. Yu, X. Zhang, F. Wang, Designing for the chemical conversion coating with high corrosion resistance and low electrical contact resistance on AZ91D magnesium alloy, Corros. Sci. 135 (2018) 197–206.
[42] Z. Chunyan, L. Shangju, Y. Baoxing, L. Xiaopeng, C. Xiao-Bo, Z. Tao, W. Fuhui, Ratio of total acidity to pH value of coating bath: a new strategy towards phosphate conversion coatings with optimized corrosion resistance for magnesium alloys, Corros. Sci. 150 (2019) 279–295.
[43] H. Huang, F. Bu, Galvanic corrosion of electronic material copper coupled silver-coating in electronic systems, Anti-Corrosion Methods Mater. 66 (2019) 730–745.
[44] Z.F. Yin, M.L. Yan, Z.Q. Bai, W.Z. Zhao, W.J. Zhou, Galvanic corrosion associated with SM 80SS steel and Ni-based alloy G3 couples in NaCl solution, Electrochim. Acta 53 (2008) 6285–6292.
[45] X.C. Zhao, S.F. Dong, B. Ge, B.X. Huang, J. Ma, H. Chen, X.H. Hao, C.Z. Wang, Effects of temperature and voltage on formation of electrolysis induced chemical conversion coating on titanium surface, Surf. Coat. Technol. 354 (2018) 330–341.